Appl Microbiol Biotechnol (2001) 56:93–100
DOI 10.1007/s002530100613

ORIGINAL PAPER

E. Jonsbu · B. Christensen · J. Nielsen

Changes of in vivo fluxes through central metabolic pathways during the production of nystatin by *Streptomyces noursei* in batch culture

Received: 18 October 2000 / Revised: 6 December 2000 / Accepted: 8 December 2000 / Published online: 26 April 2001

Abstract The central carbon metabolism of the nystatin-producing strain *Streptomyces noursei* ATCC 11455 was evaluated by ^{13}C-labelling experiments. A batch fermentation was examined during the idiophase by GC-MS measurements of the labelling patterns of amino acids in the biomass. The labelling patterns of the amino acids and calculated fluxes of the central metabolism showed that changes in the primary and secondary metabolisms occurred simultaneously. Changes in the profiles for the integrated fluxes showed a decreased flux through the pentose phosphate pathway and an increased flux in the tricarboxylic acid cycle relative to the glucose uptake rate when the culture entered a phase with reduced specific growth rate and enhanced nystatin yield. The flux through the pentose phosphate pathway seemed to be adjusted according to the NADPH requirement during the different phases of the batch fermentation.

Introduction

The secondary metabolite nystatin, which is produced by *Streptomyces noursei*, is a commercial product with a world market estimated to be in the range of U.S. $ 250–300 million year^{-1}. Nystatin belongs to the polyene macrolide antibiotics, a subgroup of the polyketides. It has antifungal activity through binding to sterols in cell membranes and thereby affecting the permeability, leading to leakage of intracellular compounds (Chambers and Sande 1995). Nystatin is effective in vitro against a large number of pathogenic and non-pathogenic fungi, but has no effect against some of the common bacteria (Gil and Martin 1997). Today, nystatin is mainly used for topical treatment of candidiasis (Bennett 1995). Until recently, polyene antibiotics were used as antifungal agents only, but several functions have now been assigned to polyenes, such as immunostimulatory drugs, insecticides and application in AIDS-related infections (Gil and Martin 1997).

Nystatin has a lactone ring of 37 carbon atoms that contains a characteristic diene–tetraene chromophore (Martin 1977). The synthesis of the Lactone ring starts with acetyl-CoA and proceeds with elongation of 15 malonyl-CoA and three methylmalonyt-CoA (Brautaset et al. 2000). One mycosamine is linked to the lactone ring, probably during secretion of the antibiotic (Gil and Martin 1997). It has been suggested that biosynthesis of the precursors takes place by non-specific methylmalonyl carboxyltransferase from oxaloacetate to acetyl-CoA/propionyl-CoA in cooperation with phosphoenolpyruvate carboxylase for regeneration of oxaloacetate (Rafalski and Raczyńska-Bojanowska 1972, 1973, 1975). An alternative pathway for the synthesis of methylmalonyl-CoA is through rearrangement of succinyl-CoA by methylmalonyl-CoA mutase, which was proved for the synthesis of erythromycin by *S. erythreus* (Hunaiti and Kolattukudy 1984). The polyketide chains of polyene macrolide antibiotics are synthesised by a large, type I, multifunctional polyketide synthase, where each active site carries out one reaction in the assembly of precursors and modification of the growing carbon chain (Gil and Martin 1997).

Although Hazen and Brown (1950, 1951) discovered nystatin as the first macrolide antifungal antibiotic almost 50 years ago, little is known about the relation between the primary and secondary metabolisms during the production of nystatin. Recently, a physiological characterisation of nystatin production demonstrated a correla-

E. Jonsbu (✉)
Department of Biotechnology,
Norwegian University of Science and Technology, NTNU,
N-7491 Trondheim, Norway
e-mail: einar.jonsbu@alpharma.no
Tel.: +47-22529268, Fax: +47-22522949

B. Christensen · J. Nielsen
Center for Process Biotechnology, BioCentrum-DTU,
Technical University of Denmark, Building 223,
DK-2800 Lyngby, Denmark

Present addresses: E. Jonsbu, Alpharma AS, Harbitzalléen 3,
N-0212 Oslo, Norway

B. Christensen, Novozymes A/S, Novo Allé 2,
DK-2880 Bagsværd, Denmark

tion between specific growth rate and the production of nystatin, with increasing productivity at decreasing specific growth rates (Jonsbu et al. 2000). The same study showed a positive influence of ammonium limitation on nystatin productivity. Physiological studies like those described above have been based on extracellular measurements of substrate consumption and the formation of products and metabolites during fermentation processes. Such a survey of fermentation processes can be combined with stoichiometric models for the intracellular reaction network; and thus mass balances over intracellular metabolites can be used to quantify the intracellular fluxes (Nielsen 1998). This technique is known as metabolic flux analysis (MFA) and the concept has been illustrated by Daae and Ison (1999), who constructed a stoichiometric model for the intracellular reactions in *S. lividans*. Using this approach, they analysed the influence exerted on the calculated fluxes by perturbations in metabolism and biomass composition. Oxygen utilisation turned out to have the highest influence on the pathway fluxes, while perturbation in the biomass composition did not significantly alter the flux pattern (Daae and Ison 1999). In another study, metabolite balancing was combined with experimental data from chemostat cultures with an actinorhodin-producing strain of *S. coelicolor*; and the intracellular flux distribution was calculated under various conditions (Naeimpoor and Mavituna 2000). Production of actinorhodin was shown not to have a significant effect on the intracellular fluxes. The model indicated that the highest actinorhodin production rate was under nitrogen limitation, but this was accompanied by an undesirable excretion of other metabolites.

Metabolic network analysis (MNA) represents a further improvement of MFA, where metabolite balancing and labelling experiments are combined to enable a more detailed analysis, including flux estimation, identification of the network structure and subcellular compartmentation (Christensen and Nielsen 1999a). Estimation of pathway fluxes by a combination of metabolite balancing and labelling experiments has been performed in several microorganisms, such as *Ashbya gossypii* (de Graaf et al. 2000), *Aspergillus niger* (Schmidt et al. 1999; Pedersen et al. 2000), *A. oryzae* (Schmidt et al. 1998), *Bacillus subtilis* (Sauer et al. 1997), *Corynebacterium glutamicum* (Marx et al. 1996, 1999), *Escherichia coli* (Fiaux et al. 1999; Sauer et al. 1999) and *Penicillium chrysogenum* (Christensen and Nielsen 2000; Christensen et al. 2000). MNA measures the labelling patterns of amino acids in biomass grown on a ^{13}C-labelled substrate. The labelling patterns of the amino acids reflect the labelling of intermediates in the central carbon metabolism and thereby the fluxes throughout the various branches of the metabolic network. Labelling patterns of amino acids have been determined from continuous cultures at steady state (Marx et al. 1996; Sauer et al. 1999; Schmidt et al. 1999; Christensen and Nielsen 2000) and in the exponential growth phase of batch fermentations, which also represents a physiological steady state (de Graaf et al. 2000; Pedersen et al. 2000). Furthermore, examination of metabolic fluxes during batch cultivation was performed by labelling experiments from three identical batch fermentations of *E. coli*, which were harvested at different times: mid-exponential phase, late exponential phase and stationary phase (Sauer et al. 1999). Due to the fact that most industrial fermentation processes are based on batch or fed-batch fermentations, it is of interest to be able to determine the metabolic flux distribution in these two types of cultivation. When metabolic shifts occur during a batch cultivation, the labelling patterns of amino acids do not reflect the in vivo fluxes at a specific time, but rather provide an integral value of the metabolic fluxes. Measurements of the labelling patterns will, however, give valuable information about the nature of the alterations in the metabolic fluxes. This study examines metabolic interactions between the primary and secondary metabolisms during the production of nystatin by *S. noursei* in a batch cultivation using ^{13}C-labelled glucose as the sole carbon source. The changes in the metabolic fluxes were assessed using data from the GC-MS measurements of the amino acid labelling patterns as input to a mathematical framework described previously (Christensen and Nielsen 2000).

Materials and methods

Microorganism

S. noursei ATCC 11455 was obtained from the American Type Culture Collection. The bacterium was inoculated into 50 ml of medium containing 37.0 g tryptic soy broth l^{-1} (Difco) and 7.0 g glucose l^{-1} and was cultured in a 300-ml shake flask with baffles for 30 h at 30 °C and 150 rpm. To this culture, 15% (v/v) glycerol was added and the culture was then stored at –80 °C. The frozen stock culture suspension was used as inoculum for seed cultures for fermentation experiments.

Fermentation

The seed culture was prepared by inoculation of 0.5 ml of stock culture into 50 ml of the seed medium FD-1. The seed cultures were incubated in 300-ml shake flasks with baffles and 50 glass beads (diameter: 3 mm) for 25 h at 30 °C and 250 rpm. FD-1 was a chemically defined medium containing (per litre): 8.0 g glucose, 4.5 g $(NH_4)_2SO_4$, 2.0 g KH_2PO_4, 1.0 g $MgSO_4 \cdot 7H_2O$, 21.0 g Mops (3-*N*-morpholinepropanesulfonic acid) and 3 ml TMS-1 (trace metal solution). Glucose and TMS-1 were added after sterilisation and the pH of the medium was aseptically adjusted to 7.0. TMS-1 consisted of (per litre): 5.0 g $FeSO_4 \cdot 7H_2O$, 390 mg $CuSO_4 \cdot 5H_2O$, 440 mg $ZnSO_4 \cdot 7H_2O$, 150 mg $MnSO_4 \cdot H_2O$, 10 mg $NaMoO_4 \cdot 2H_2O$, 20 mg $CoCl_2 \cdot 2H_2O$ and 50 ml 37% HCl.

Production fermentations were carried out in a 450-ml bioreactor with a working volume of 200 ml. The bioreactor was made of glass and especially designed to prevent wall growth. The defined production medium contained (per litre): 12.5 g [1-^{13}C]glucose (Omicron Biochemicals), 12.5 g unlabelled glucose, 8.3 g $(NH_4)_2SO_4$, 1.5 g KH_2PO_4, 1.0 g $MgSO_4 \cdot 7H_2O$ and 3 ml TMS-1. The bioreactors were inoculated with 5.0 ml of seed culture. The pH of the cultures was controlled to 6.5 by the addition of 2 M NaOH and the temperature was kept at 28 °C. Air was supplied to the headspace of the bioreactor and sparged into the culture; and the dissolved oxygen concentration in the culture was monitored. The supplied air was bubbled through 2 N NaOH to strip off atmospheric CO_2. The 2 N NaOH was replaced by dis-

tilled water for the first 20 h of the fermentation to ensure the admission of CO_2 for cell growth.

Samples of 12 ml were taken during the fermentation. Dry weight measurements of biomass were performed from fresh fermentation samples. Triplicate samples of 2 ml were centrifuged (10,000 *g*, 5 min, 4 °C). The supernatant and biomass pellets were immediately frozen at –20 °C for later analysis.

Analysis

Dry weight of biomass

For dry weight measurements, 5 ml of the culture was filtered through a pre-dried filter (Supor-450, 0.20 µm, Gelman Laboratories), washed with 10 ml distilled water and dried to constant weight at 105 °C.

Glucose, acetate and pyruvate

Supernatant from the medium was analysed by an isocratic HPLC method using a HPX-87H aminex ion-exclusion column (7.8×300 mm, BioRad). The column was eluted at 60 °C with 5 mM H_2SO_4 at a flow rate of 0.6 ml min^{-1}. The detectors were a Waters 410 refractive index detector and a Waters 486 tunable absorbence detector (210 nm).

Ammonium

The concentration of ammonium in the supernatant of the medium was measured using an ion-selective ammonia electrode (Metrohm) with ammonium chloride as the standard.

Nystatin

Nystatin was extracted from the fermentation broth by adding dimethylformamide to fresh culture samples in the ratio 1:1. The solution was mixed for 10 min and biomass was then removed by centrifugation (5,000 *g*, 10 min). The extract was stored at –20 °C. For HPLC measurements of nystatin, a Hewlett Packard instrument (series 1100) with a reversed phase Waters Symmetry column (C-18, 4 µm particles, 4.6×150 mm) and UV detector (295 nm) was used. The column was kept at 25 °C. An isocratic method was used for the mobile phase with a flow rate of 1.0 ml min^{-1}. The eluent consisted of 0.05 M ammonium acetate (pH 3.8) mixed with acetonitrile in the ratio 3:2. The injection volume of samples and standards (4,670 USP units mg^{-1}, Sigma) was 20 µl and the run time was 10 min.

Amino acid derivatives for GC-MS

The method of Christensen and Nielsen was used (1999b). Biomass pellets from 2-ml samples were hydrolysed using 6 M HCl at 105 °C for 20 h. The hydrolysate was filtered (0.45 µm) and evaporated at 105 °C. For derivatisation with ethylchloroformate (ECF), dried hydrolysate was dissolved in 600 µl 20 mM HCl and 400 µl pyridine:ethanol (1:4) was added. The mixture was derivatised by adding 50 µl ECF, and the derivatives were extracted into 1 ml dichloromethane. The organic phase was removed for analysis on GC-MS. For derivatisation with (*N*,*N*)-dimethylformamide dimethyl acetal (DMFDMA), dried hydrolysate was dissolved in 100 µl methanol and 200 µl acetonitrile was added. The mixture was derivatised by adding 600 µl DMFDMA.

Glucose pentaacetate for GC-MS

Crude biomass from 2-ml samples was hydrolysed using 6 M HCl at 105 °C for 20 min. Hydrolysate (100 µl) was derivatised by adding 1.0 ml acetic anhydride and 50 µl acetyl choride. The derivatives were stored at room temperature for 24 h and analysed by GC-MS.

Gas chromatography–mass spectrometry

The GC-MS analysis of the amino acid derivatives is described by Christensen and Nielsen (1999b). Glucose pentaacetate was analysed on the GC-MS using an initial oven temperature of 130 °C for 3 min. Hereafter, the temperature was raised with a gradient of 20 °C min^{-1} until a temperature of 280 °C was reached. This temperature, 280 °C, was held for 8 min. The flow through the column was held constant at 0.9 ml He min^{-1}. The injection volume was 2 µl. Temperature at the inlet was 270 °C. The quadrupole temperature was 105 °C.

Results

Fermentation profile

The fermentation profiles for the batch culture are given in Fig. 1. The fermentation was divided into two phases: an initial phase of nystatin production, P1, and a second production phase, P2. P2 represented a transient phase for the specific growth rate and two time periods, P2a

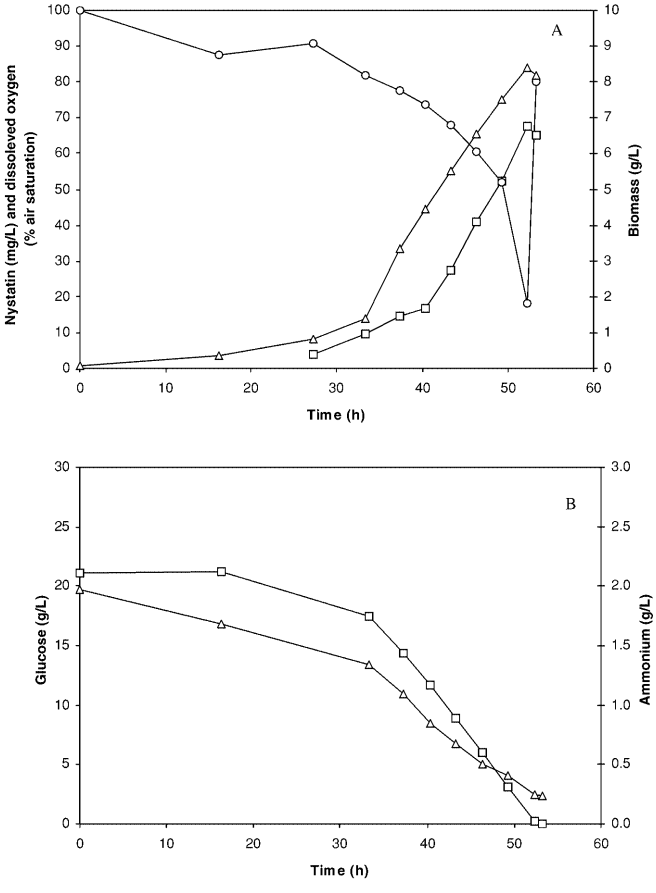

Fig. 1A, B Batch culture of *Streptomyces noursei*. **A** Cell growth (△), nystatin production (□) and dissolved oxygen tension (○) during fermentation. **B** Concentration of ammonium △) and glucose (□) during fermentation

Table 1 Specific cell growth, specific uptake rate of glucose, specific production rate of nystatin and nystatin yield from biomass. *DW* Dry weight of biomass

Parameters	Phase P1	Phase P2a	Phase P2b
Time (h)	27–37	40	52
μ (h^{-1})	0.140	0.082	0.034
r_s (g glucose g^{-1} DW h^{-1})	0.25	0.21	0.11
r_p (mg nystatin g^{-1} DW h^{-1})	0.59	0.86	0.61
$Y_{xp, nys}$ (mg nystatin g^{-1} DW)	4.3	10.4	18.0

and P2b, were therefore considered. Calculated data for specific growth rates, specific uptake rates of glucose, specific production rates of nystatin and nystatin yields on biomass are summarised in Table 1.

The growth pattern initially showed exponential growth. The average specific growth rate during the initial production phase of nystatin, P1, was more than 70% higher than the corresponding value in phase P2a or P2b. A 2- to 4-fold increase in the nystatin yields occurred after 40 h of fermentation, marking the beginning of the second production phase, P2. There was no limitation of glucose, ammonium or oxygen during the fermentation.

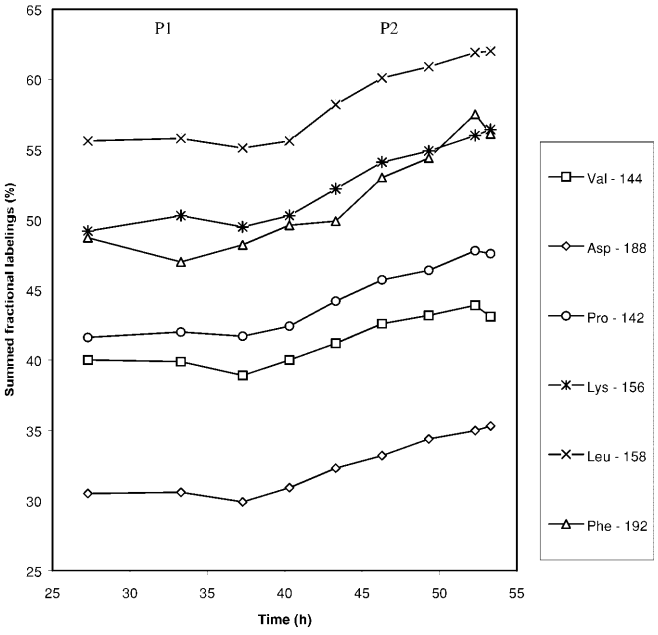

Fig. 2 Summed fractional labelling of amino acids during batch fermentation of *S. noursei*.

Labelling patterns of amino acids

The labelling patterns of the amino acids were described by the summed fractional labelling of the fragments arising from the ionisation process taking place in the MS. The summed fractional labelling of a fragment was defined as the sum of the fractional labellings of the carbon positions in the fragment, as described by Christensen and Nielsen (2000). Figure 2 illustrates the variations of the summed fractional labellings from these amino acid fragments throughout the cultivation. The general trend showed nearly constant labelling patterns of the amino acid fragments until the specific growth rate decreased at the end of the P1 phase. This was followed by an approximately linear increase during the P2 phase, which was characterised by having an increased nystatin production. The changes in the labelling patters of the amino acids reflected changes in the central carbon metabolism from the time the specific growth rate decreased and the nystatin production rate increased. A reduction of the pentose phosphate pathway flux (PPP-flux) was indicated by the increase in the fragment valine-144, which represented the labelling fraction of the 2nd and 3rd pyruvate position.

Integrated flux estimation

The labelling patterns of protein-bound amino acids constitute the basis for flux estimation; and, since the labelling pattern of the protein pool changes relatively slowly to the time-scale of physiological responses, an error occurs when making flux estimations of batches with non-constant physiological behaviour. However, in a batch cultivation, the labelling pattern of protein formed after a metabolic shift will eventually be reflected in the labelling patterns of the combined pools of “old” and “new” protein. To investigate the characteristics of the change in metabolism taking place at the transition from the phase P1 to phase P2, flux estimations were performed irrespective of the difficulties associated with basing the calculations on a combined pool of protein. Thus the fluxes were calculated as if the labelling patterns were the result of a constant metabolism. Since these fluxes were not identical to the in vivo fluxes calculated from, e.g. steady state cultures, the term “integrated fluxes” was chosen for the fluxes calculated using this procedure. Consequently, the integrated fluxes are simply reflecting tendencies in the metabolism, e.g. a decrease in the PPP-flux; and they should not be interpreted as actual in vivo fluxes at a specific time-point. The estimation of the integrated net fluxes was performed as previously described for the determination of in vivo fluxes under steady state conditions (Christensen and Nielsen 2000), where the biomass yield from each sample was taken into consideration in the stoichiometric model. The integrated fluxes were estimated as an average of nine estimations. All integrated fluxes were normalised with respect to the specific glucose uptake rate, where the integrated flux from glucose to glucose-6-phosphate was set to 100.

As revealed by the labelling patterns of the amino acids, the integrated fluxes of the central carbon metabolism at the transition from high specific growth rates and low nystatin production changed to low specific growth rates and high nystatin production. Three integrated fluxes related to branch points in the central carbon metabolism were especially found to vary during phase P2: the PPP-flux

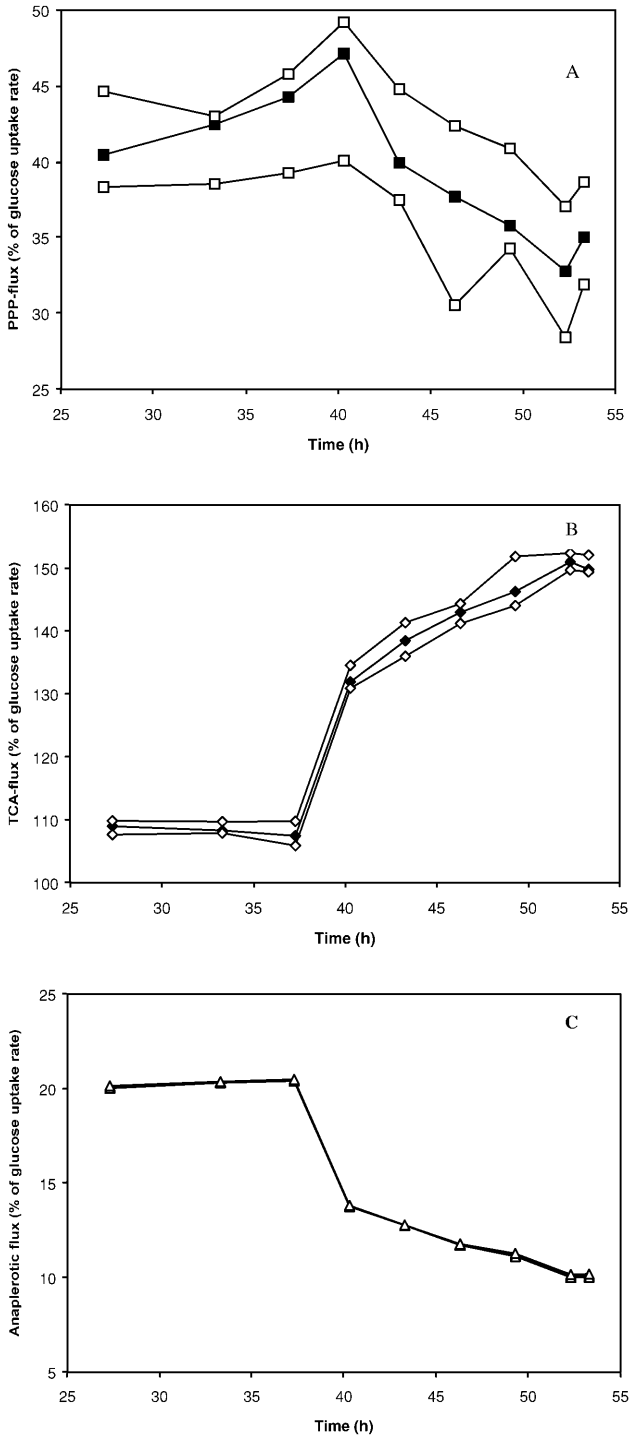

Fig. 3A–C Integrated fluxes through the central carbon metabolism. **A** Integrated flux in pentose phosphate pathway. ■ Average flux, from nine estimates, □ maximum and minimum values of estimated fluxes. **B** Integrated flux in tricarboxylic acid cycle. ■ Average flux, from nine estimates, □ maximum and minimum values of estimated fluxes. **C** Integrated anaplerotic flux. ■ Average flux, from nine estimates, □ maximum and minimum values of estimated fluxes

(Fig. 3A), the tricarboxylic acid (TCA)-flux (Fig. 3B) and the anaplerotic flux from pyruvate to oxaloacetate (Fig. 3C). The integrated PPP-flux increased from about 40 to 47 and then dropped to about 33 during phase P2, with

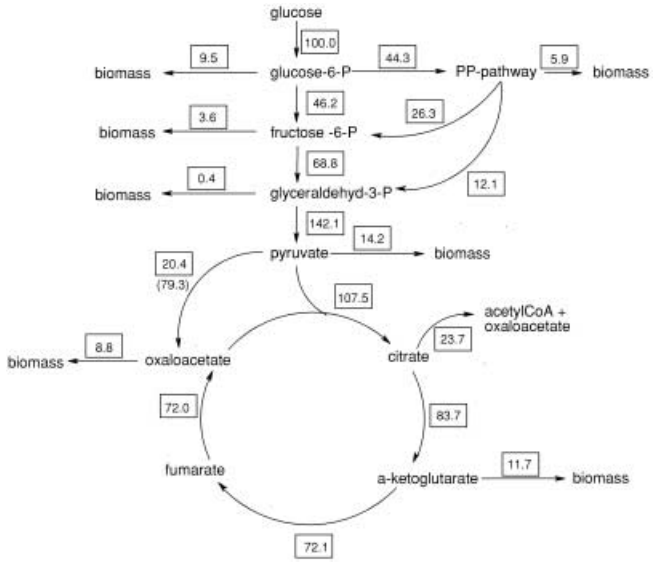

Fig. 4 Estimated in vivo fluxes at the end of phase P1. All fluxes are normalised with respect to the glucose uptake, which was set to 100. The value in parenthesis denotes the reverse exchange flux between pyruvate and oxaloacetate

enhanced nystatin production. The integrated fluxes of the TCA cycle and the anaplerotic pathway were constant in phase P1, followed by an increase of about 40% and a reduction of about 50% during phase P2, respectively.

Exponential specific growth rate and linear profile of nystatin production during phase P1 implied conditions of balanced growth; and the integrated fluxes at the end of phase P1 therefore represented the in vivo fluxes during this phase. The integrated fluxes of the main pathways in the central metabolism at the end of phase P1 are shown in Fig. 4. The calculation of the integrated fluxes was based on the summed fractional labelling data given in Table 2. The branch point between the PPP and the Embden–Meyerhof–Parnas (EMP) pathway displayed an almost equal flux distribution through these two pathways. The flux from oxaloacetate to pyruvate represented the sum of all conversions of C-4 compounds in the TCA cycle to C-3 compounds in the EMP pathway, as is usual in this type of analysis (Marx et al. 1996; Sauer et al. 1997; Christensen and Nielsen 2000).

NADPH requirement

The NADPH requirements for cell growth and nystatin production were evaluated. The evaluation was based on an assumption of similar NADPH requirements for cell growths for *P. chrysogenum* and *S. noursei*, where the *P. chrysogenum* NADPH requirement was taken to be 8.5 mmol NADPH g^{-1} dry weight in a defined medium (Nielsen 1997). The synthesis of amino acids constituted more than 95% of the total NADPH requirement for cell growth. NADPH was also necessary as reductive power for the biosynthesis of nystatin through the keto-reduction and enoyl-reduction of β-keto groups of C_2 units be-

Table 2 Summed fractional labellings of biomass components at the end of phase P1. In the "intermediates", phosphoenolpyruvate and pyruvate were treated as one metabolite in the calculations. The "carbon atoms" refer to the intermediate carbon positions present in the ion. Some of the measured components consist of carbon atoms from two different intermediates. In these cases, the numbers in parentheses refer to the carbon atoms of the intermediates in parentheses. *Acetyl-CoA* acetyl coenzyme A, *DMFDMA* (*N*,*N*)-dimethyl-formamide dimethyl acetal, *ECF* ethylchloroformate, *Erythrose-4-P* erythrose-4-phosphate, *Glucose-6-P* glucose-6-phosphate

Derivatised component	Derivatisation agent	Ion cluster (*m*/*z*)	Intermediate	Carbon atoms	Summed fractional ^{13}C labellings
Glucose	–	331	Glucose-6-P	1, 2, 3, 4, 5, 6	55.4
Glycine	ECF	175	Glycine	1, 2	2.8
Glycine	DMFDMA	144	Glycine	1, 2	2.1
Glycine	DMFDMA	85	Glycine	2	1.1
Serine	ECF	174	Serine	1, 2	1.0
Serine	ECF	132	Serine		17.7
Alanine	ECF	116	Pyruvate	2, 3	19.7
Alanine	DMFDMA	99	Pyruvate	2, 3	20.0
Alanine	DMFDMA	158	Pyruvate	1, 2, 3	21.9
Leucine	ECF	158	Acetyl-CoA and (pyruvate)	2, (2), (2), (3), (3)	55.1
Valine	ECF	144	Pyruvate	2, 2, 3, 3	38.9
Valine	DMFDMA	143	Pyruvate	1, 2	5.6
Valine	DMFDMA	127	Pyruvate	2, 2, 3, 3	39.1
Aspartate	ECF	188	Oxaloacetate	2, 3, 4	29.9
Aspartate	DMFDMA	115	Oxaloacetate	2	9.0
Aspartate	DMFDMA	216	Oxaloacetate	1, 2, 3, 4	34.5
Threonine	ECF	175	Oxaloacetate	1, 2	13.4
Glutamate	DMFDMA	143	α-Ketoglutarate	1, 2	21.9
Glutamate	DMFDMA	230	α-Ketoglutarate	1, 2, 3, 4, 5	48.3
Proline	ECF	142	α-Ketoglutarate	2, 3, 4, 5	41.7
Lysine	ECF	156	Acetyl-CoA and (α-ketoglutarate)	2, (2), (3), (4), (5)	49.5
Phenylalanine	ECF	192	Erythrose-4-P and (pyruvate)	1, 2, 3, 4, (2), (2), (3), (3)	48.2
Phenylalanine	DMFDMA	143	Phosphoenolpyruvate	1, 2	2.4

Table 3 NADPH requirement for cell growth and nystatin production and the NADPH production in the pentose phosphate pathway (PPP) and the tricarboxylic acid (TCA) cycle

Parameters	Phase P1	Phase P2a	Phase P2b
Time (h)	27–37	40	52
$Y_{xNADPH} \cdot \mu$ (mmol NADPH g^{-1} DW h^{-1})	1.19	0.70	0.29
$Y_{pNADPH} \cdot r_p$ (mmol NADPH g^{-1} DW h^{-1})	0.024	0.035	0.025
$2\nu_{ppp} \cdot r_s$ (mmol NADPH g^{-1} DW h^{-1})	1.23[a]	1.07	0.41
$1\nu_{isocitr} \cdot r_s$ (mmol NADPH g^{-1} DW h^{-1})	1.16[b]	1.32	0.88

[a] Based on the final value for the integrated PPP-flux within the time interval
[b] Based on the final value for the integrated TCA-flux from isocitrate within the time interval

ing assembled into the polyketide chain. This NADPH requirement was calculated to be 41 mmol NADPH g^{-1} nystatin. A balance for NADPH is given in Table 3, where the NADPH requirements based on cell growth and nystatin production during phases P1 and P2 were calculated and compared with the formation of NADPH from the PPP and the TCA cycle. In the calculations, it was assumed that isocitrate dehydrogenase from the TCA cycle only used $NADP^+$ as a co-factor (Roszkowski et al. 1971). Cell growth represented the major part of the NADPH requirement, although the relative requirement to fulfil nystatin production increased 2- to 4-fold from phase P1 to P2 and constituted between 5% and 8% of the total NADPH requirement in phase P2.

Discussion

A shift in the production of nystatin, with a 2- to 4-fold increased yield, occurred between phases P1 and P2, where the specific growth rate decreased. Such a change in nystatin production agreed with the correlation between increased nystatin productivity at decreased specific growth rates found in a previous study (Jonsbu et al. 2000). The same study demonstrated the positive effect of ammonium depletion, which was observed as an increase in nystatin production when cultures became ammonium-limited. Neither ammonium nor other measured substrates (glucose and oxygen) came into limitation in the fermentation reported here; and therefore this could not explain the increase in nystatin production. The profile of this fermentation had a longer phase of exponential growth before reaching a transition state and a longer lag-phase for the production of nystatin than observed earlier (Jonsbu et al. 2000). This may be a consequence of reducing the inoculum size from the 5% used in the previous study to 2.5%, as the performance of a microbial culture can be strongly influenced by the size and age of the inoculum (Elibol et al. 1995).

At present, the macromolecular composition of *Streptomyces* spp is not available. Estimation of the integrated fluxes was therefore based on the cell composition of *P. chrysogenum* (Nielsen 1997). However, sensitivity analysis of a model for flux calculation of the metabolic pathways in *S. lividans* demonstrated that a 20% change in the demand for any building blocks did not affect the flux pattern significantly (Daae and Ison 1999).

The changes in the labelling patterns of amino acids when the nystatin yield increased indicates that the primary and secondary metabolisms are linked. This was further confirmed by the profiles of the estimated integrated fluxes of the PPP, the TCA cycle and the anaplerotic pathway from pyruvate to oxaloacetate, which all changed significantly when the specific growth rate decreased and nystatin production increased. However, the cause of the metabolic changes and how the primary and secondary metabolisms interact is unknown. Based on the results, three suggestions can be made about a possible relation between the primary and the secondary metabolism. Genetic control, possibly by global regulation, or by environmental conditions of the culture, might have: (1) influenced the primary and the secondary metabolism simultaneously, (2) influenced the primary metabolism, which had direct impact on the secondary metabolism, or (3) changed the secondary metabolism, thus causing the primary metabolism to support/maintain this change.

The requirement for NADPH was calculated to be more than two-fold higher in phase P1 compared to phase P2, mainly due to a lower specific growth rate in the P2. However, the formation of NADPH was still found to be in excess in both phases. These calculations were based on the formation of 2 mol NADPH mol^{-1} glucose-6-phosphate entering the PPP and 1 mol NADPH mol^{-1} isocitrate being converted to α-ketoglutarate in the TCA cycle. *Streptomyces* spp are generally known to have NADPH-dependent glucose-6-phosphate dehydrogenase activity only, but *S. aureofaciens* was shown to exhibit activity with both NAD-linked and NADP-linked glucose-6-phosphate dehydrogenase (Neužil et al. 1988). No NAD(P) dependent trans-hydrogenase activity was detected in *S. noursei* ATCC 21581, producing the nystatin variant polifungin (Roszkowski et al. 1971). The decrease in the integrated PPP-flux in phases P1 and P2 lowered the formation of NADPH. It seemed as if the PPP-flux was adjusted according to the reduced requirement for NADPH in phase P2. The changes in the PPP-flux and the formation of NADPH throughout this pathway are assumed to occur more rapidly and probably by a greater effect than the calculations showed. The integrated fluxes reflected alterations slower and less decisive than in vivo fluxes. In phase P1, the formation of NADPH through the TCA cycle was in the same range as that formed in the PPP, whereas the TCA cycle contributed relatively more to the formation of NADPH in phase P2. There was an increase in the relative integrated TCA-flux in P2, even though the total NADPH requirement for cell growth and nystatin production dropped. The TCA cycle has been reported to be an important source for the generation of NADPH; and Roszkowski et al. (1971) found isocitrate dehydrogenase to be the most active NADP-dependent dehydrogenase system in *S. noursei* ATCC 21581 and *S. erythreus*.

Examination of integrated fluxes in the central carbon metabolism, by combining labelling experiments and metabolite balancing, showed a trend for a decreasing PPP-flux, from 47 to 33 when the culture reached the transition to a lower specific growth rate and enhanced nystatin productivity. Sensitivity analysis of a stoichiometric model designed for *S. lividans* demonstrated that specific growth rates affected the calculated fluxes; and it was shown that an increase in the specific growth rate diverted the glucose catabolism from the EMP pathway to the PPP (Daae and Ison 1999).

The integrated flux from oxaloactate to pyruvate included the collection of all fluxes from C-4 intermediates in the TCA cycle to C-3 metabolites in the EMP pathway. Several enzymes may contribute to this flux: oxaloacetate decarboxylase, malic enzyme, phosphenolpyruvate carboxykinase and also methylmalonyl carboxyltransferase, which was suggested to be the enzyme responsible for the formation of malonyl-CoA and methylmalonyl-CoA, the precursors for the biosynthesis of nystatin (Rafalski and Raczyńska-Bojanowska 1972, 1975). This integrated flux was almost four times higher than the net flux from pyruvate to oxaloacetate. The flux distribution pattern obtained in chemostat cultures of *P. chrysogenum* showed an anaplerotic pathway flux from pyruvate to oxaloacetate equal to the integrated flux we calculated; but, in contrast to our results, the reverse flux was in the same order as the anaplerotic flux (Christensen and Nielsen 2000).

Acknowledgements This work was financed by Alpharma and the Norwegian Research Council and was supported by a grant from the Nordic Network on Physiological Engineering (NordPhys). We thank T.E. Ellingsen and O.-M. Gulliksen for valuable comments on this manuscript.

References

Bennett JE (1995) Antimicrobial agents, antifungal agents. In: Hardman JG, Goodman Gilman A, Limbird LE (eds) The pharmacological basis of therapeutics, 9th edn. McGraw-Hill, New York, pp 1175–1188

Brautaset T, Sekurova ON, Sletta H, Ellingsen TE, Strøm AR, Valla S, Zotchev SB (2000) Biosynthesis of the polyene antifungal antibiotic nystatinin Streptomyces noursei ATCC 11455: analysis of the gene cluster and deduction of the biosynthetic pathway. Chem Biol 7: 395–403

Chambers HF, Sande MA (1995) Antimicrobial agents, general considerations. In: Hardman JG, Goodman Gilman A, Limbird LE (eds) The pharmacological basis of therapeutics, 9th edn. McGraw-Hill, New York, pp 1029–1042

Christensen B, Nielsen J (1999a). Metabolic network analysis: a powerful tool in metabolic engineering. Adv Biochem Eng Biotechnol 66:209–231

Christensen B, Nielsen J (1999b) Isotopomer analysis using GC-MS. Metabol Eng 1:282–290

Christensen B, Nielsen J (2000) Metabolic network analysis of *Penicillium chrysogenum* using ^{13}C-labelled glucose. Biotechnol Bioeng 68:252–259

Christensen B, Thykær J, Nielsen J (2000) Metabolic characterization of high- and low-yielding strains of *Penicillium chrysogenum*. Appl Microbiol Biotechnol 54:212–217

Daae EB, Ison AP (1999) Classification and sensitivity analysis of a proposed primary metabolic reaction network for *Streptomyces lividans*. Metabol Eng 1:153–165

Elibol M, Ulgen K, Kamaruddin K, Mavituna F (1995) Effect of inoculum type on actinorhodin production by *Streptomyces coelicolor* A3(2). Biotechnol Lett 17:579–582

Fiaux J, Andersson CIJ, Holmberg N, Bülow L, Kallio PT, Szyperski T, Bailey JE, Wüthrich K (1999) ^{13}C NMR flux ratio analysis of *Escherichia coli* central carbon metabolism in microaerobic bioprocesses. J Am Chem Soc 121:1407–1408

Gil JA, Martin JF (1997) Polyene antibiotics. In: Strohl WR (ed) Biotechnology of antibiotics. Decker, New York, pp 551–575

Graaf AA de, Mahle M, Möllney M, Wiechert W, Stahmann P, Sahm H (2000) Determination of full ^{13}C isotopomer distributions for metabolic flux analysis using heteronuclear spin echo difference NMR spectroscopy. J Biotechnol 77:25–35

Hazen El, Brown R (1950) Two antifungal agents produced by a soil actinomycete. Science 122: 423

Hazen, EL, Brown R (1951) Fungicidin, an antibiotic produced by a soil actinomycete. Proc Soc Exp Biol Med 76:93–97

Hunaiti AA, Kolattukudy PE (1984) Source of methylmalonyl-coenzyme A for erythromycin synthesis: methylmalonyl-coenzyme A mutase from *Streptomyces erythreus*. Antimicrob Agents Chemother 25:173–178

Jonsbu E, Ellingsen TE, Nielsen J (2000) Effects of nitrogen sources on cell growth and production of nystatin by *Streptomyces noursei*. J Antibiot 53:1354–1362

Martin JF (1977) Biosynthesis of polyene macrolide antibiotics. Annu Rev Microbiol 31:13–38

Marx A, Graaf AA de, Wiechert W, Eggeling L, Sahm H (1996) Determination of the fluxes in the central metabolism of *Corynebacterium glutamicum* by nuclear magnetic resonance spectroscopy combined with metabolite balancing. Biotechnol Bioeng 49:111–129

Marx A, Eikmanns BJ, Sahm H, Graaf AA de, Eggeling L (1999) Response of the central metabolism in *Corynebacterium glutamicum* to the use of an NADH-dependent glutamate dehydrogenase. Metabol Eng 1:35–48

Naeimpoor F, Mavituna F (2000) Metabolic flux analysis in *Streptomyces coelicolor* under various nutrient limitations. Metabol Eng 2:140–148

Neužil J, Novotná J, Erban V, Behal V, Hošt'álek Z (1988) Glucose-6-phosphate dehydrogenase from tetracycline producing strain of *Streptomyces aureofaciens*: some properties and regulatory aspects of the enzyme. Biochem Int 17:187–196

Nielsen J (1997) Primary metabolism. In: Nielsen J (ed) Physiological engineering aspects of *Penicilium chrysogenum*. World Scientific, London, pp 63–138

Nielsen J (1998) Metabolic engineering: techniques for analysis of targets for genetic manipulations. Biotechnol Bioeng 58:125–132

Pedersen H, Christensen B, Hjort C, Nielsen J (2000) Construction and characterization of an oxalic acid non-producing strain of *Aspergillus niger*. Metabol Eng 2:34–41

Rafalski A, Raczyńska-Bojanowska K (1972) Synthesis of malonate and methylmalonate and the formation of polyene antibiotics. Acta Biochem Pol 19:71-87

Rafalski A, Raczyńska-Bojanowska K (1973) Biochemical criteria in selection of high productive strains of *Streptomyces noursei* var. *polifungini*. Acta Biochem Pol 5:87–93

Rafalski A, Raczyńska-Bojanowska K (1975) Non-specific acetyl-CoA carboxylase and methylmalonyl-CoA carboxyltransferase in *Streptomyces noursei* var. *polifungini*. Acta Biochem Pol 22:311–317

Roszkowski J, Ruczaj Z, Sawnor-Korszyńska D, Kotiuszko D, Morawska H, Siejko D, Raczyńska-Bojanowska K (1971) NAPDH-regenerating systems in microorganisms producing macrolide antibiotics. Acta Microbiol Pol Ser B 3:97–106

Sauer U, Hatzimanikatis V, Bailey JE, Hochuli M, Szyperski T, Wüthrich K (1997) Metabolic fluxes in riboflavin-producing *Bacillus subtilis*. Nat Biotechnol 15:448–452

Sauer U, Lasko DR, Fiaux J, Hochuli M, Glaser R, Szyperski T, Hatzimanikatis T, Wüthrich K, Bailey J E (1999) Metabolic flux ratio analysis of genetic and environmental modulations of *Eschericha coli* central carbon metabolism. J Bacteriol 181:6679–6688

Schmidt K, Marx A, Graaf AA de, Wiechert W, Sahm H, Nielsen J, Villadsen J (1998) ^{13}C tracer experiments and metabolite balancing for metabolic flux analysis: comparing two approaches. Biotechnol Bioeng 58:254–257

Schmidt K, Nørregaard LC, Pedersen B, Meissner A, Duus JØ, Nielsen J (1999) Quantification of intracellular metabolic fluxes from fractional enrichment and ^{13}C–^{13}C coupling constraints on the isotopomer distribution in labelled biomass components. Metabol Eng 1:166–179